Petroleum Science 20 (2023) 2468–2478

Contents lists available at ScienceDirect

Petroleum Science

journal homepage: www.keaipublishing.com/en/journals/petroleum-science

Original Paper

Pre-heating temperature induced flowability and wax deposition characteristics of crude oil adding wax inhibitors

Bo Yao [a, b, *], Hao-Ran Zhu [c], Bao-Dong Yan [d], Chuan-Xian Li [a], Fei Yang [a], Guang-Yu Sun [a], Hong-Bo Zeng [b, **]

[a] College of Pipeline and Civil Engineering, China University of Petroleum, Qingdao, Shandong, 266580, People's Republic of China
[b] Department of Chemical and Materials Engineering, University of Alberta, Edmonton, AB, T6G 1H9, Canada
[c] School of Petroleum Engineering, Changzhou University, Changzhou, Jiangsu, 213164, People's Republic of China
[d] China Oil & Gas Pipeline Network Corporation, Beijing, 100020, China

ARTICLE INFO

Article history:
Received 31 October 2022
Received in revised form
24 February 2023
Accepted 24 February 2023
Available online 27 February 2023

Edited by Jia-Jia Fei

Keywords:
Pre-heating treatment
Wax inhibitor
Flowability
Wax deposition
Waxy crude oil

ABSTRACT

This paper investigated the effects of pre-heating treatment temperatures (T_{pre}) on the flowability and wax deposition characteristics of a typical waxy crude oil after adding wax inhibitors. It is found that there is little difference in wax precipitation exothermic characteristics of crude oils at different T_{pre}, as well as the wax crystal solubility coefficient in the temperature range of 25–30 °C. For the undoped crude oil, the flowability after wax precipitation gets much improved and the wax deposition is alleviated as T_{pre} increasing. At T_{pre} = 50 °C, the viscosity and wax deposition rate of crude oil adding wax inhibitors are higher than those of the undoped crude oil. When the T_{pre} increases to 60, 70, and 80 °C, the flowability of the doped crude oil are largely improved and the wax deposition is suppressed with the T_{pre} increase, but the wax content of wax deposit increases gradually. It is speculated that, on the one hand, the T_{pre} increase helps the dispersion of asphaltenes into smaller sizes, which facilitates the co-crystallization with paraffin waxes and generates more aggregated wax crystal flocs. This weakens the low-temperature gel structure and increases the solid concentration required for the crosslink to form the wax deposit. On the other hand, the decrease in viscosity increases the diffusion rate of wax molecules and accelerates the aging of wax deposits. The experimental results have important guiding significance for the pipeline transportation of doped crude oils.

1. Introduction

Waxy crude oil is an important fossil energy source, which contains a large number of paraffin waxes. Paraffin waxes mainly refer to normal alkanes with 16–35 carbon atoms (Aiyejina et al., 2011). It dissolves as molecules in the crude oil at high temperatures, but as the temperature decreases, the solubility of wax molecules in the crude oil gradually decreases. And the wax molecules crystallize out into solid wax crystal particles when the oil temperature is lower than the wax appearance temperature (WAT) (Chala et al., 2018). The precipitated wax crystals may accumulate and lead to the flowability deterioration of oil (Sousa et al., 2020). Also, the dissolved wax components in crude oil may diffuse to the pipe wall and deposits on the pipe wall together with other components (such as resins, asphaltenes, sands, etc.) in the crude oil, which reduces the circulation area and transport capacity of the pipeline (Yang et al., 2020; Giacchetta et al., 2019; Leporini et al., 2019). To explain the wax deposition phenomenon, scholars have proposed a variety of wax deposition mechanisms, including molecular diffusion, Brownian diffusion, shear dispersion, gravity sedimentation, thermal diffusion, etc. (Ragunathan et al., 2020). It is generally believed that molecular diffusion is the dominant mechanism for the wax deposition process (Singh et al., 2000). Many corresponding wax deposition models have been established, and the influence of crude oil composition (Fan et al., 2021), flow rate (Kang et al., 2019), temperature (Janamatti et al., 2019), time (Mansourpoor et al., 2019), tube wall material (Li R. et al., 2021) and other factors on the wax deposition process were studied. In practice, both mechanic pigging and chemical prevention are often

* Corresponding author. College of Pipeline and Civil Engineering, China University of Petroleum, Qingdao, Shandong, 266580, People's Republic of China.
** Corresponding author.
E-mail addresses: ybcy2013@sina.com (B. Yao), Hongbo.Zeng@ualberta.ca (H.-B. Zeng).

https://doi.org/10.1016/j.petsci.2023.02.030

used to alleviate wax deposition problems, ensuring the economic and safe operation of oil pipelines and preventing pipeline blockage accidents (Sousa et al., 2019).

Pre-heating treatment was found effective in Chinese waxy oilfields early in the 1980s. An appropriate pre-heating temperature can help waxy crude oil to gain improved low-temperature flowability and inhibit wax deposition. Evdokimov et al. (2003) from Russia reported that a kind of Russian waxy crude oil exhibits an abnormal pour point when the pre-heating temperature is different. Xu and Huang (2010) found that the preheat treatment may improve or strengthen the structure of wax crystals in the oil, and different preheat-treatment temperatures to some degree dictate a better or worse rheological property of waxy crude oil. Zhu et al. (2018) found that there are significant differences in the thickness and composition of wax deposits in Changqing crude oil when pre-heated to different temperatures. Zhu pointed out that the optimal pre-heating temperature can disperse the asphaltenes in crude oil, and the dispersed asphaltenes can significantly modify the wax crystal morphology, thereby improving the low-temperature rheological (reducing the apparent viscosities in the non-Newtonian temperature rage) and wax deposition characteristics.

Adding polymeric wax inhibitors can generally enhance the flowability of waxy crude oil (Chi et al., 2016), reduce the wax deposition rate, and increase the wax content of the wax deposit layer (Chi et al., 2017). The wax inhibitors mainly interact with paraffin wax through eutectic, nucleation, and adsorption to improve the wax crystal morphology (Sousa et al., 2019; Li W. et al., 2021). The efficiency of wax inhibitors is also related to wax deposition conditions such as oil temperature, wall temperature, flow rate, and wax deposition time. It is believed that polymeric wax inhibitors are effective at lower oil temperatures below WAT, but are invalid at higher temperatures. Qing and Lei (2004) found that the wax deposition rate of the doped crude oil in the high-temperature range was lower than that of the undoped crude oil. And in the low-temperature range, the wax inhibitor did not inhibit the wax deposition, and the amount of wax deposition increased instead. Jennings and Weispfennig (2005) reported that with the increase in shear stress, the performance of wax inhibitors gradually showed an upward trend. Chi et al. (2016) found that the efficiency of wax inhibitors changes significantly with the development of wax deposition time, so wax deposition time needs to be considered when choosing wax inhibitors. Researchers not only study the influence of wax inhibitors on wax deposition but also pay attention to some changes in wax deposit properties brought by wax inhibitors. At present, it has been generally recognized that adding wax inhibitors will increase the wax content of the wax deposit (Jafari Ansaroudi et al., 2013; Wang et al., 2003; Yang et al., 2021). Yang et al. (2016) added asphaltenes to waxy oil and found that a small number of asphaltenes would cause a heterogeneous wax deposit structure. They added a certain amount of polyoctadecyl acrylate (POA) to waxy oil and found that the wax deposit changed from a homogeneous to a heterogeneous wax deposit structure, which proved that POA participates in the wax deposition process (Yang et al., 2018). Recently, Yao et al. (2018) developed a kind of composite wax inhibitor based on amino-functionalized polymethylsilsesquioxane (PAMSQ) microsphere and found that after the amino-functionalization, the flow-improving efficiency of composite wax inhibitor is further enhanced than that of polyethylene vinyl acetate (EVA). Further, they carried out the wax deposit experiments by adding EVA/PAMSQ (Yao et al., 2018b), and the results showed that the wax deposit mass of crude oil treated with EVA/PAMSQ is reduced compared to the untreated oil and the oil treated with EVA. And for the untreated crude, the strong gel structural strength of the oil is responsible for the wax deposition, and the formed wax deposit is like the gelled oil; For the treated oil, the reduced apparent viscosities increased the wax content of the initial deposit and facilitated the wax diffusion.

In this paper, the main goal is to study the effect of pre-heating treatment on the wax deposit properties of waxy crude oil adding wax inhibitor. Firstly, by adding the EVA/PAMSQ composite wax inhibitors, the crystallization exothermic, rheological, and microscopic properties of crude oils at different pre-heating temperatures were investigated. Then, the wax deposition experiments for all the doped oil samples were carried out to study the deposit mass, appearance, and deposit rate of wax deposition. Finally, both the experimental and theoretical methods were applied to discuss the mechanism of pre-heating and chemical treatment.

2. Materials and methods

2.1. Materials

2.1.1. Characteristics of waxy crude oil

As illustrated in Table 1, the waxy crude oil used here was provided by Changqing oilfield in China (Chang5 layer in Mahuangshan district) and is mainly composed of saturates (68.65 wt%) and aromatics (21.71 wt%). The carbon number distribution of crude oil is shown in Fig. 1.

2.1.2. EVA/PAMSQ wax inhibitor

The melt blending method was adopted to prepare the EVA/PAMSQ wax inhibitor. During the melt blending process, the mass ratio of EVA wax inhibitor and the PAMSQ microsphere is controlled at 20:1. EVA was purchased from Aladdin Biotechnology Co., Ltd. The vinyl acetate (VA) content and the melt index of the EVA wax inhibitor are 28% and 6 g/10min, respectively. The relative molecular weight is about 20,000 g/mol. The heat flow curve in the crystallization process of EVA wax inhibitor is shown in Fig. 2, which shows the initial crystallization temperature at 59 °C and the peak crystallization temperature at 49 °C.

The doped crude oil is prepared by adding 50 ppm EVA/PAMSQ wax inhibitors into the Changqing waxy crude oil at different T_{pre} of 50, 60, 70, or 80 °C.

2.2. Methods

In this paper, we first investigated the crystalline exothermic properties of waxy oils using the highly accurate DSC method and explained the thermal dynamics of waxy oils affected by the pre-heat temperatures. The morphologies of waxy oils at a low temperature were presented as well. Then, the rheological behaviors were studied through the static oscillation and dynamic cooling process, where Arrhenius activation energy, gelation point, viscoelasticity parameters were analyzed. At last, wax deposition experiments were carried out by applying self-patented wax deposit device, where the mass evolution, wax content, composition, appearance and distribution of wax deposit were studied clearly.

Table 1
Physical properties of Changqing crude oil.

Saturates	Aromatics	Resins	Asphaltenes	Wax content	ρ_4^{20}
68.65 wt%	21.71 wt%	8.11 wt%	1.53 wt%	21.1 wt%	0.880

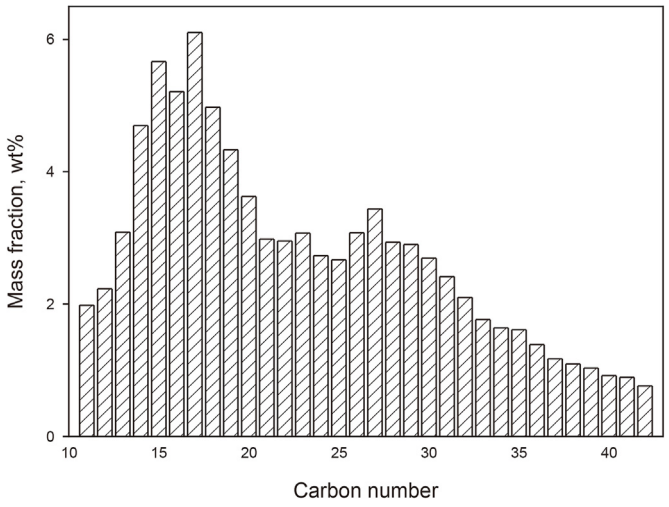

Fig. 1. Carbon number distribution of Changqing waxy crude oil.

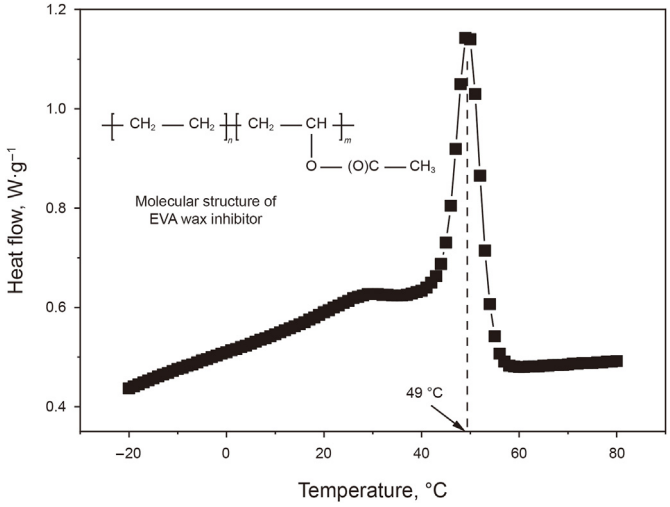

Fig. 2. Heat flow curve of EVA wax inhibitor during the cooling process.

We finally concluded the mechanism of pre-heat temperature upon the flowability and deposition characteristics.

DSC test. The DSC821^e differential scanning calorimeter (Mettler-Toledo Co., Switzerland) was adopted to test the wax precipitation characteristics of the crude oil and wax deposit samples. The test sample was first heated to T_{pre} and then was cooled to −25 °C at a fixed cooling rate of 5 °C/min. During the cooling process, the temperature and the heat flow were recorded. When the sample temperature is higher than the wax appearance temperature (T_w), the heat flow temperature curve is a straight baseline. The WAT is identified to be the highest temperature that deviates from the baseline during the cooling process. The precipitated wax amount is calculated through Eq. (1) (Martos et al., 2008).

$$W = \frac{\int_T^{T+dT} \frac{[q(T) - q_b(T)]}{R_c} dT}{\overline{Q}} \times 100\% \quad (1)$$

where, W is the precipitated wax amount in the temperature range of $T \sim T + dT$, wt%; $q(T)$ and $q_b(T)$ are the heat flow per unit mass sample and the baseline heat flow, respectively, and R_c is the cooling rate, °C/min; $\overline{Q}$ is the average crystallization heat of wax, the value of which used here is 220 J/g.

Microscopic observation. The crude oil sample was first heated to T_{pre} and then cooled at a cooling rate of 0.5 °C/min. By using the Olympus BX51 polarizing microscope (Olympus Co., Japan), the microscopic morphology of the precipitated wax crystal particles can be photographed under polarized light. The observation temperature was chosen as 15 °C.

Flow curve and small amplitude oscillation shearing. The coaxial cylinder measurement system of DHR-1 rheometer (TA Co., America) was used to measure the flow characteristics of crude oil. The crude oil was firstly pre-heated and then statically cooled to 10 °C at a cooling rate of 0.5 °C/min, during which the viscosity was measured at a constant shear rate of 50 s^{-1}. When testing the small-amplitude oscillation shear characteristics of crude oil, a small-amplitude oscillating shear with a frequency of 1 Hz and a strain of 0.0005 was applied during the cooling process from 50 °C to 10 °C.

Pour point test. After different pre-heating, the pour points of crude oils were measured according to the Chinese standard SY/T 0541-2009.

Wax deposition experiment. The self-developed Couette wax deposition experimental device was adopted to carry out the wax deposition experiments. The structure diagram of the device is shown in Fig. S1 of the supporting information. It is mainly composed of a wax deposition cylinder, a sample cylinder, and a hot/cold water bath. The wax deposition cylinder is connected to the cold-water bath to simulate the inner wall of the pipeline. The sample cylinder can contain oil samples, and the outer wall of the sample cylinder is connected to the hot-water bath. The outer wall of the sample cylinder represents the center of the oil flow in the pipeline. The sample cylinder can be driven by a servo motor. After pre-heating, the oil sample is placed in a cold-water bath and cooled to the experimental oil temperature at a cooling rate of 0.5 °C/min. Then the oil sample was poured into the sample cylinder. The wax deposition time is set as 1 h, 3 h, 6 h, 12 h, and 24 h, and just after that, the wax deposition cylinder can be raised by the lifting system. At this time, the wax deposits can be scraped off and weighed. A small amount of surface and bottom layer wax deposits are sampled with a sampling spoon for subsequent analysis.

HTGC test. The Varian 3800 GC gas chromatography and STAR workstation were used to perform gas chromatography analysis to obtain the carbon number distribution of crude oil and wax deposit samples. The injection volume is set to 0.4 μL, the injection port temperature is 320 °C, and the initial column temperature is 50 °C. After 5 min of constant temperature, the temperature is increased to 320 °C at a rate of 8 °C/min, and then the temperature is kept constant for 30 min. The carbon number distribution can be obtained by analyzing the experimental data, which is detailed found in reference (Ruwoldt et al., 2019).

3. Results and discussion

3.1. DSC

The DSC curves and wax crystal solubility coefficients of crude oils at different T_{pre} are shown in Fig. 3(a) and (b). Here, the reproducibility of temperature and heat flow is less than 0.1 °C and 0.1 W/mg. It can be seen that the DSC curves of crude oil samples all show two exothermic peaks around 35 °C and 20 °C. The effect of T_{pre} on the wax precipitation process of the doped crude oil can be ignored. The T_w at $T_{pre} = 50$ °C is 39.6 °C, while it slightly decreases to just less than 39 °C as T_{pre} increases to 60, 70, and 80 °C. According to Eq. (1), the calculated precipitated wax amounts

at −20 °C at T_{pre} = 50, 60, 70, and 80 °C are 18.6, 18.5, 18.6, and 18.7 wt%, respectively. As illustrated in Fig. 1(b), when the temperature is lower than 20 °C, the wax crystal solubility coefficients of the doped crude oils show a slightly increasing trend with T_{pre} increase. However, the wax crystal solubility coefficients basically do not change with T_{pre} increase around 25 °C. Compared to the data reported in previous articles (Ruwoldt et al., 2019; Kurniawan et al., 2021; Dorsman et al., 2022), the different T_{pre} may affect the initial interactions around the T_w where the paraffin waxes start to precipitate with wax inhibitors, indicating that the good dispersion state of polymers facilitates the wax inhibitors to take effects. Here, we must mention that the cooling rate used here is a specific choice that cannot reflect the non linear correspondence of T_w with cooling rate, and Ruwoldt et al. (2018) have conducted a comprehensive work upon this point.

3.2. Microscopic morphology

In Fig. 4, for the undoped oil samples, the wax crystals at T_{pre} = 50 °C showed a fine and dispersed state; when T_{pre} was increased to 60 °C, there was no significant change in the morphology of wax crystals, and when T_{pre} was increased to 70 °C, the wax crystals showed a dispersed and broken spherical aggregating morphology; At T_{pre} = 80 °C, the agglomeration and size of crude oil wax crystals further increased, but the morphology did not change significantly. For the doped oil samples, at T_{pre} = 50 °C, the wax crystals of crude oil are the same as the undoped one; by contrast, once T_{pre} increases higher than 60 °C, the morphologies of wax crystals change significantly. At T_{pre} = 50 °C, the dispersed wax crystals agglomerate together to form clusters, and the size of the wax crystal aggregations increase a lot; when T_{pre} = 70 °C and 80 °C, this agglomeration effect is further enhanced gradually, and the size of the clusters of wax crystals continues to increase, which agree with the findings in references (Zhao et al., 2021; Makwashi et al., 2021).

3.3. Flowability

3.3.1. Viscosity-temperature relation

The viscosity-temperature curves of undoped and doped crude oils at different T_{pre} are shown in Fig. 5. The reproducibility of viscosity and temperature is less than 1 mPa s and 0.1 °C. At T_{pre} = 50 °C, the apparent viscosities of doped crude oil increased slightly compared to that of undoped crude oil. When T_{pre} increases to 60, 70, and 80 °C, the wax inhibitor exhibits a viscosity reducing effect. Taking 25 °C as an example, the viscosity of the undoped crude oil at T_{pre} = 60, 70, and 80 °C is 540.7, 380.2, and 83.1 mPa s, respectively, and the viscosity of the doped crude oil is reduced to 43.2, 38.2 and 39.5 mPa s, respectively, with the viscosity reduction rate of 92%, 90% and 52%, respectively. Among them, the viscosity reduction rate at T_{pre} = 60 °C is the highest.

Furthermore, flow curves above 40 °C (higher than WAT of all the crude oil samples) were applied to calculate the apparent Arrhenius activation energy (U_{app}) for all the undoped/doped samples. Results shown in Fig. 6 indicate that U_{app} of the doped crude oil at the same T_{pre} is slightly higher than that of undoped crude oil. By definition, U_{app} alters the formation/deformation of internal bonds for dispersants in crude oil. As the temperatures range beyond WAT, U_{app} is actually indicative of the interactions between asphaltenes/resins and wax inhibitors. The oil sample at T_{pre} = 50 °C possesses the highest U_{app} around 19 kcal/mol, which is located in the range of 14–20 kcal/mol that is reported for the asphaltene activation/association energies (Wong and Yen, 2000). As T_{pre} increases, U_{app} of undoped/doped crude oil exhibits a decreasing trend, meaning that the structures of associated asphaltenes/wax inhibitors are easier to be destroyed, which is in accord with the data tested by the impedance spectroscopy (Chen et al., 2019).

3.3.2. Small amplitude oscillation shearing

The small-amplitude oscillation characteristics of undoped and doped crude oils at different T_{pre} are shown in Fig. 7. The gel point of the undoped crude oil is 26.7 °C at T_{pre} = 50 °C. As T_{pre} is increased to 60, 70, and 80 °C, the gel point changed to 27.6, 26.4, and 21.9 °C, respectively. For the doped samples, the gel point decreases from 29.7 °C to 9.4 °C with T_{pre} increasing from 50 to 60 °C. When T_{pre} is higher than 70 °C, the gel point can decrease to be lower than 5 °C. A great difference in the values of storage/loss modulus at the same temperature can also be found between the undoped and doped oil samples. At T_{pre} = 50 °C, the doped crude oil has only slightly lower storage/loss modulus values than those of the undoped, but possesses a higher gel point, indicating that the added wax inhibitors cannot improve the flowability of oil at T_{pre} = 50 °C. When T_{pre} is above 60 °C, the gel point and storage/loss modulus of the doped crude oil are significantly lower than those of the undoped crude oil.

3.3.3. Pour point

The pour points of undoped/doped crude oil were also tested here and shown in Table 2. The deviation of pour point is 1–2 °C. When T_{pre} increases from 50 °C to 70 °C, the pour point of undoped crude oil only decreased by 3 °C, and when T_{pre} continues to increase to 80 °C, the pour point of the crude oil significantly decreased by 8 °C. In comparison, the effect of pre-heating treatment temperature on the pour point of the doped crude oil is particularly obvious. The pour point of doped crude oil at

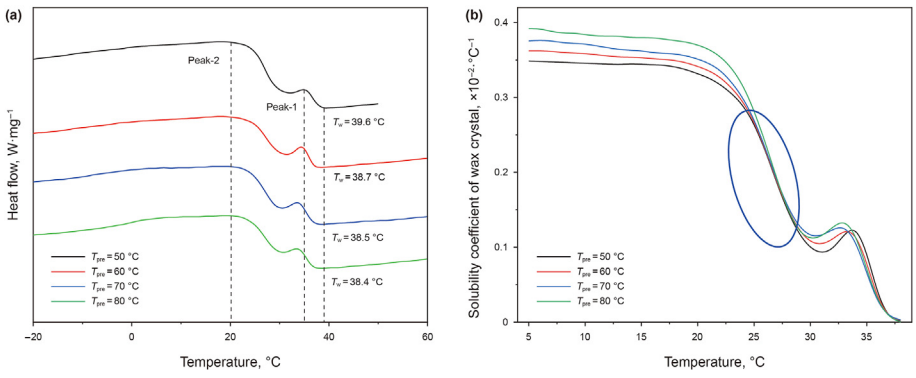

Fig. 3. DSC curves (**a**) and wax crystal solubility coefficients (**b**) of crude oils at different T_{pre}.

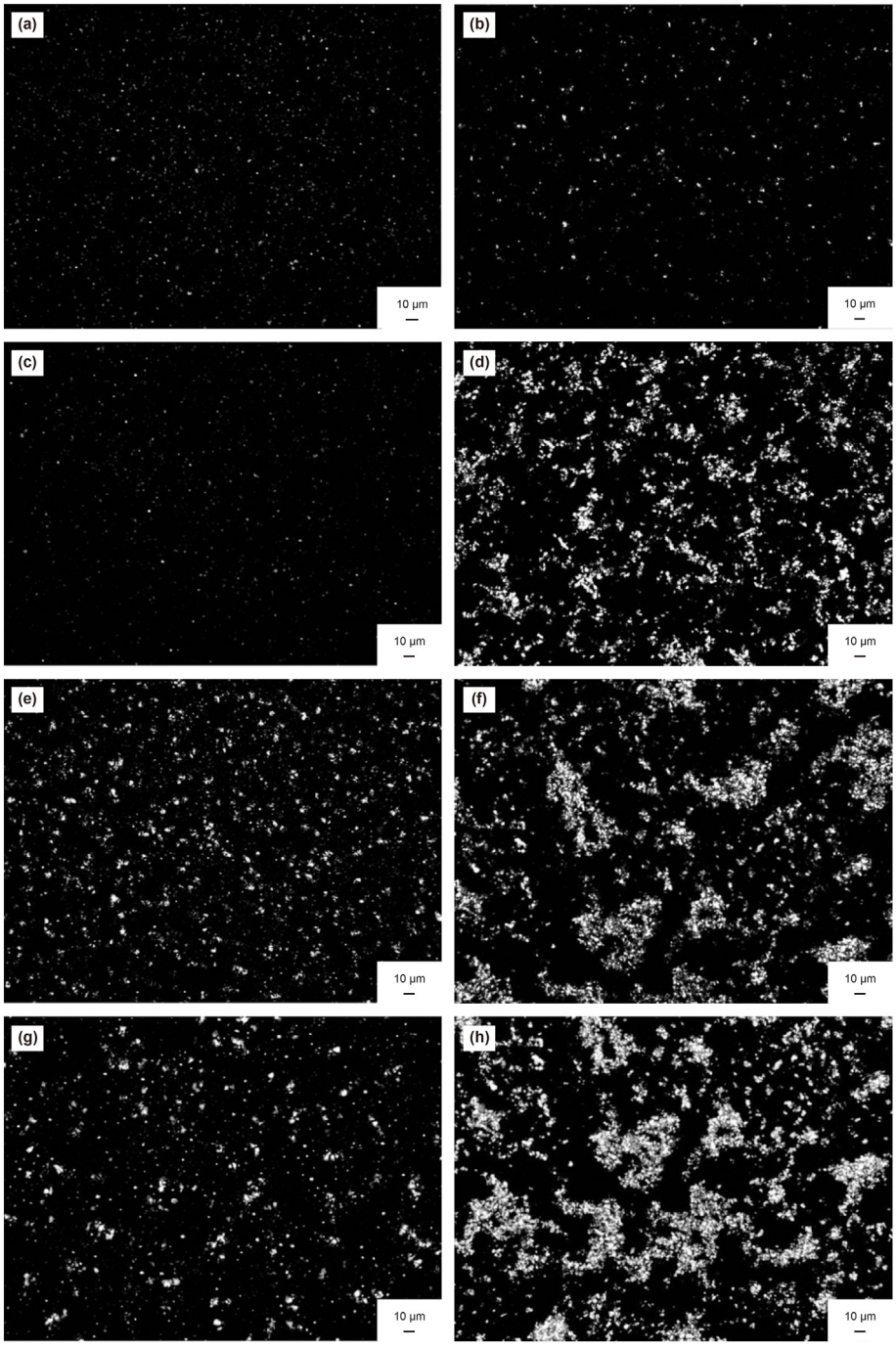

Fig. 4. Micromorphology of wax crystals of crude oil at different T_{pre}: (**a**) undoped, 50 °C; (**b**) doped, 50 °C; (**c**) undoped, 60 °C; (**d**) doped, 60 °C; (**e**) undoped, 70 °C; (**f**) doped, 70 °C; (**g**) undoped, 80 °C; (**h**) doped, 80 °C.

T_{pre} = 60 °C is already lower than that of the undoped crude oil at T_{pre} = 80 °C. When T_{pre} rises to 80 °C, the pour point of doped crude oil is already below 0 °C.

3.4. Wax deposition characteristics

3.4.1. Wax deposition rate

Here, the reproducibility of wax deposit mass is less than 0.2 g/dm^2. From Fig. 8(a), at T_{pre} = 50 °C, the wax deposit mass of doped crude oil is slightly higher than that of undoped crude oil, indicating that the wax inhibitor has no wax inhibition efficiency. When T_{pre} is higher than 60 °C, the wax deposit mass of undoped and doped crude oils will decrease with the increase of T_{pre}. Compared to the undoped crude oil, the wax deposit mass of the doped crude oil is significantly reduced. At T_{pre} = 60, 70, and 80 °C, the wax deposit mass of the undoped crude oil is 10.7, 2.2, 1.2 g/dm^2, and the wax deposit mass of the doped crude oil is 2.4, 1.9, 1.1 g/dm^2, and the wax inhibition efficiency is 78%, 14%, 8%, respectively. According to Fig. 5(b), the wax content of wax deposits formed by the undoped and doped crude oils increases with the increase of T_{pre}. Taking doped crude oil as an example, the average wax content of wax deposits at T_{pre} = 50 °C is 19 wt%. When T_{pre}

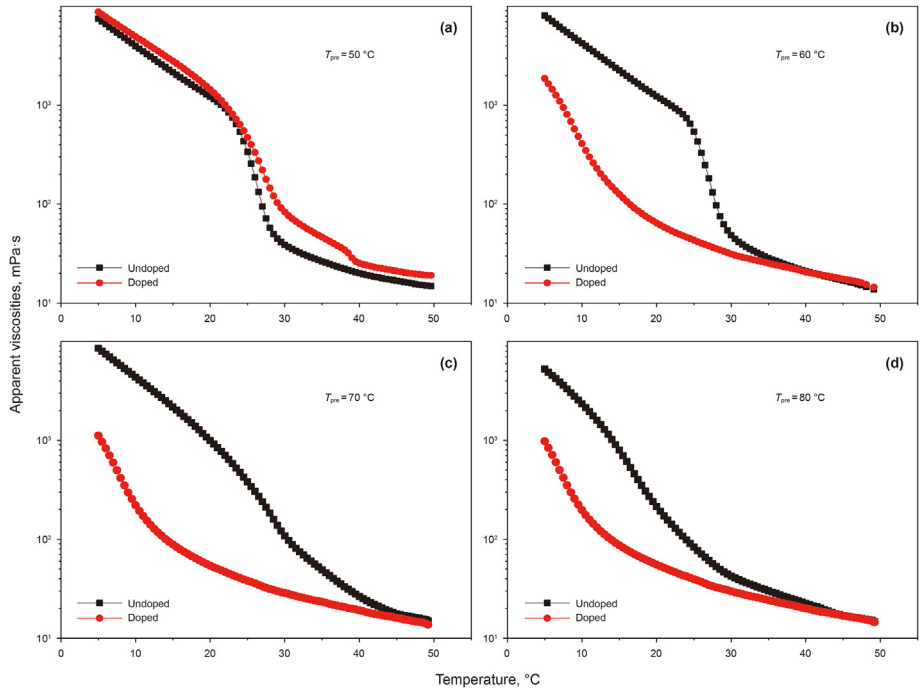

Fig. 5. The viscosity-temperature curve of undoped and doped crude oil treated at different T_{pre}: (**a**) 50 °C; (**b**) 60 °C; (**c**) 70 °C; (**d**) 80 °C.

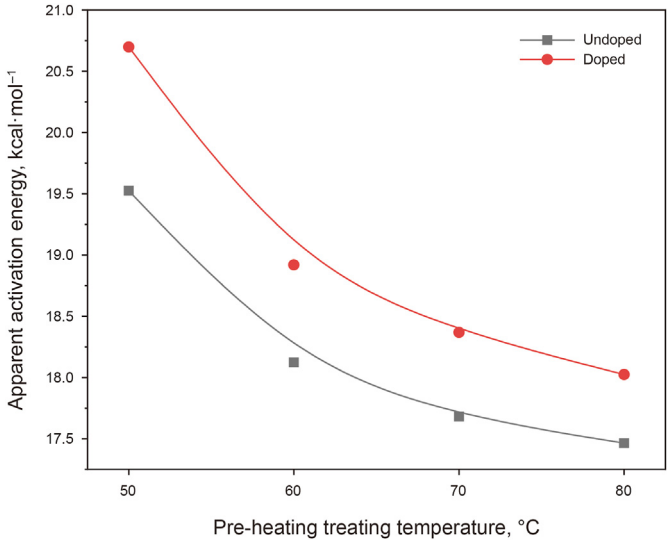

Fig. 6. Effect of T_{pre} on the apparent Arrhenius activation energy.

increases to 60, 70, and 80 °C, the average wax content of wax deposits increases to 22, 27, and 33 wt%, respectively.

As illustrated in Fig. 9, the wax deposit mass at different T_{pre} gradually increases with deposition time. Taking T_{pre} = 70 °C as an example, the wax deposit mass at 1, 3, 6, 12, and 24 h are 1.0, 1.5, 1.9, 2.2, and 2.4 g/dm^2, respectively. In terms of wax deposition rate, the wax deposition rate of 1–3 h, 3-6 h, 6-12 h, and 12-24 h are 0.25, 0.13, 0.05, and 0.01 g/(dm^2·h). It can be seen from Fig. 9 that as T_{pre} increases, the wax deposition rate decreases. Taking 6 h as an example, the wax deposit mass of the doped crude oil at T_{pre} = 50 °C is 6.2 g/dm^2. As T_{pre} gradually increases to 60, 70, and 80 °C, the wax deposit mass decreases to 2.4, 1.9, and 1.1 g/dm^2.

3.4.2. Composition and structure of the wax deposit

The composition and structure of the wax deposit formed by the doped crude oil at different T_{pre} after 6 h are shown in Figs. 10–13, respectively. The wax deposit thickness is about 3.5 mm. The WAT of the surface and bottom layer wax deposits are 37 and 38 °C, respectively. The wax content of the surface and bottom layer wax deposits are 18.8 wt% and 19.9 wt%, respectively. Therefore, the wax deposit shows a homogeneous structure.

When T_{pre} increases to 60 °C, the wax deposit thickness decreases to 1 mm. Moreover, the WATs of the surface and bottom layer wax deposits increase to 41 and 43 °C, respectively. The wax content of the surface and bottom layer wax deposits also increase to 21.4 and 24.9 wt%, respectively.

When T_{pre} increases to 70 °C, the wax deposit thickness continues to decrease to 0.5 mm. The WAT and wax content of the whole wax deposit increase to 45 °C and 26.9 wt%.

At T_{pre} = 80 °C, the wax deposit thickness is lower than 0.5 mm. The WAT and wax content of the wax deposit dramatically increase to 45 °C and 32.8 wt%.

Therefore, with the increase of T_{pre}, the wax deposit thickness gradually decreases, but the WAT and the wax content of the formed wax deposit increase. When T_{pre} is 50 °C, the wax deposit shows a homogeneous. When T_{pre} is above 60 °C, the wax deposit shows a dramatic aging rate.

3.4.3. Carbon number distribution of wax deposit

The development of the *n*-alkane composition of the wax deposits formed by the doped crude oil at different T_{pre} with time is shown in Fig. 14. At T_{pre} = 50 °C and 60 °C, the critical carbon number (CCN) of wax deposit is C_{21} and C_{22}, respectively, that is, the *n*-alkanes with carbon number > CCN continuously diffuse from the bulk oil into the wax deposit with time, while the *n*-alkanes with carbon number ≤ CCN continuously counter-diffuse from the wax deposit into the bulk oil with time. When T_{pre} increases to 70 °C and 80 °C, it increased to C_{23}, meaning that the increase of T_{pre} contributes to the rich of higher carbon number *n*-alkanes in wax deposits.

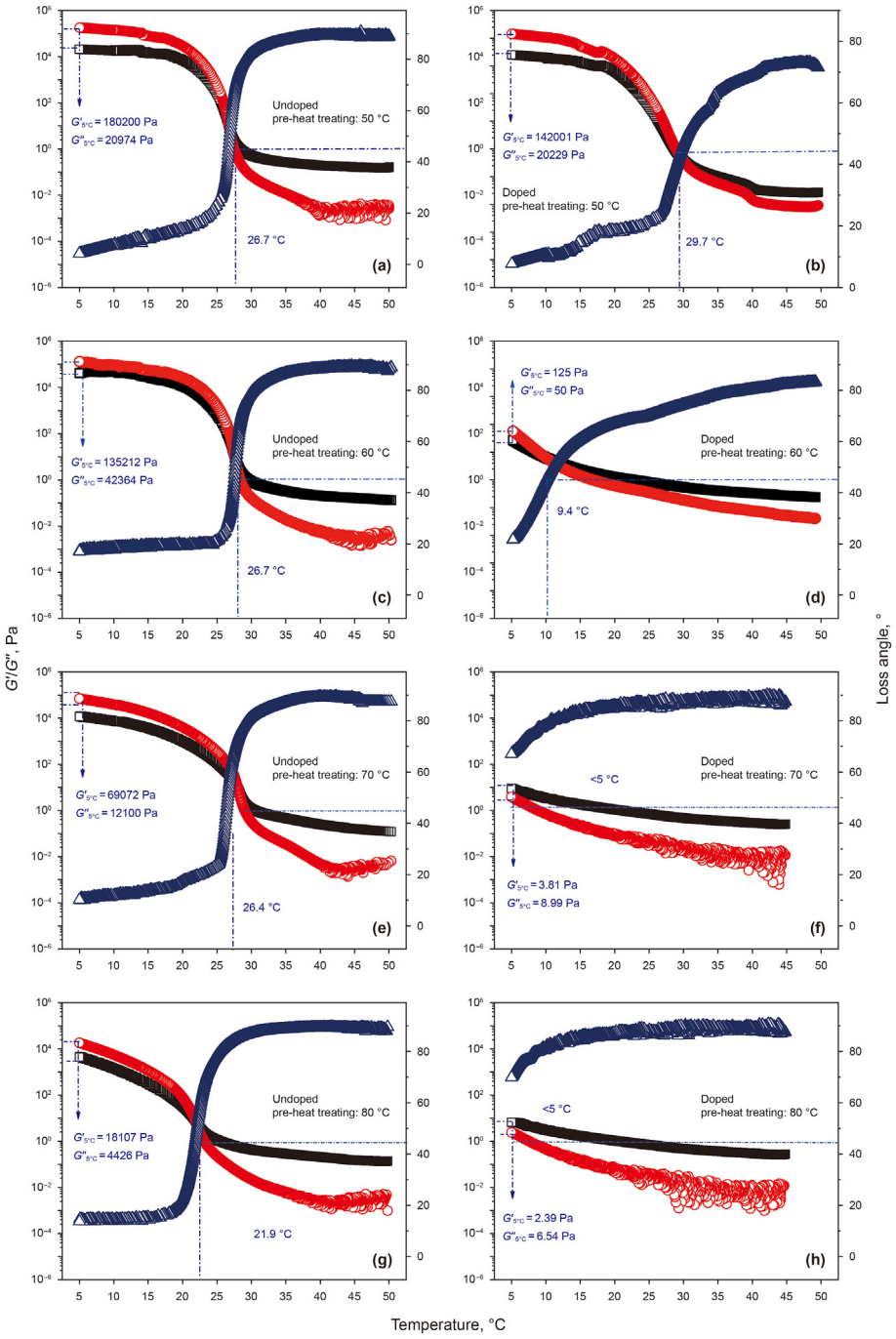

Fig. 7. G'、G'' and δ of crude oil with the temperature at different T_{pre}: (**a**) undoped oil, 50 °C; (**b**) doped oil, 50 °C; (**c**) undoped oil, 60 °C; (**d**) doped oil, 60 °C; (**e**) undoped oil, 70 °C; (**f**) doped oil, 70 °C; (**g**) undoped oil, 80 °C; (**e**) doped oil, 80 °C. (Red: storage modulus; Black: loss modulus; Blue: loss angle).

Table 2
Pour points of crude oil.

T_{pre}	50 °C	60 °C	70 °C	80 °C
Undoped	27	26	24	16
Doped	26	14	6	<0

3.5. Discussion

3.5.1. Effect of T_{pre} on the flowability of the undoped/doped crude oil

It can be seen from Section 3.2 that T_{pre} influences the low-temperature flowability (i.e. apparent viscosity, storage/loss modulus and pour point) of the undoped/doped crude oil greatly. For the undoped crude oil, the asphaltenes/resins can act as the natural pour point depressants or flow improvers, but their efficiency needs to be activated by the pre-heating treatment above a critical T_{pre}. At an appropriate T_{pre}, the bonds and interactions among asphaltene/resin aggregations are rebuilt in the solvent environment. The asphaltene/resin aggregations are dispersed into smaller sizes and lots of the saturated carbon chains in asphaltene/resin backbones are exposed in the crude. During the cooling process, more saturated carbon chains anticipate the crystallization

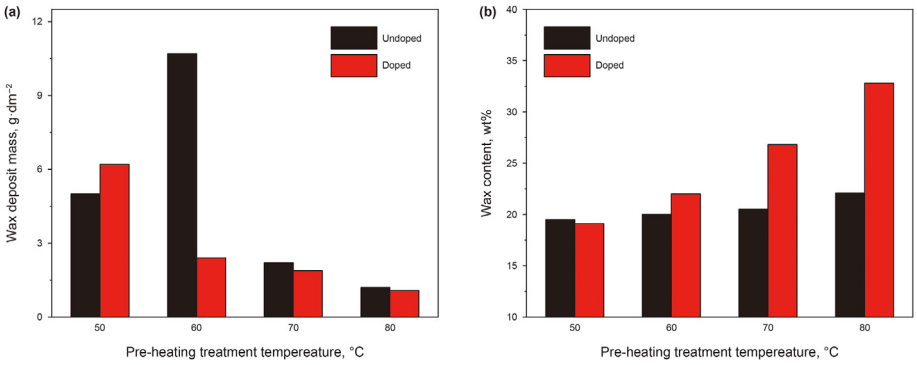

Fig. 8. Effect of T_{pre} on the mass and wax content of the wax deposit (**a**) Wax deposit mass; (**b**) Average wax content.

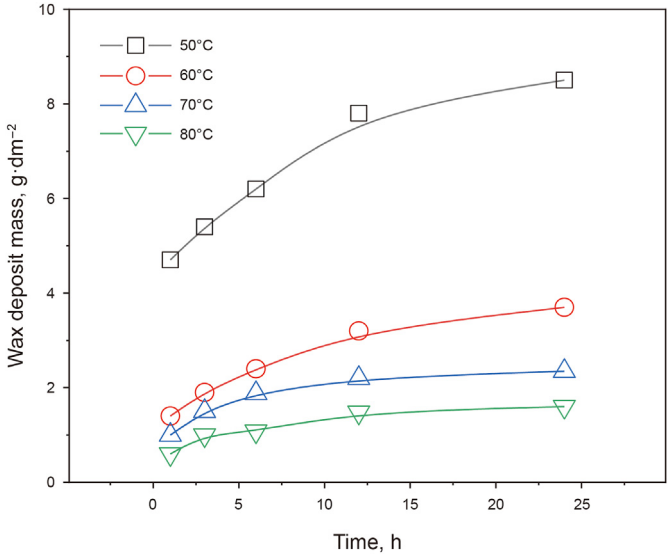

Fig. 9. The development of wax deposit mass of doped crude oil with time.

of paraffin waxes to facilitate the co-crystallization and the polar groups interfere with the growth of crystals. Therefore, the increased agglomeration and size of wax crystals with the T_{pre} increase were observed. The in-situ characterization of asphaltenes/resins in the original crude oil, however, is challenging due to the dark nature of crude oil. Here, we carried out the DLS experiments by adding toluene/heptane solutions (crude oil concentration is 10 vol%) for dilution and asphaltene destabilization (see Fig. S2 of support information file). We can clearly find that the increase of temperatures disperses the asphaltenes into smaller aggregations, which is also found in the reference (Sun et al., 2019). Future research will be carried out by our lab to study the revolution of in-situ asphaltene/resin aggregation with temperatures and the critical dispersion state of asphaltenes/resins that is beneficial to interact with paraffin waxes.

For the doped crude oils, the active components above WAT include asphaltenes/resins, wax inhibitors, and solvents. At T_{pre} = 50 °C, neither wax inhibitors nor asphaltenes/resins can disperse completely in crude oils, that is, the functional groups cannot stretch fully in the solvation environment, thereby the limited improvement of doped crude oil flowability after paraffin wax precipitation is achieved. As T_{pre} increases, the solvation effect is strengthened and the asphaltenes/resins and wax inhibitors are better dispersed for stronger interactions between wax inhibitors and asphaltenes/resins. As discussed in previous works (Yao et al., 2018a; Yao et al., 2018b), the asphaltenes and EVA/PAMSQ can form the EVA/PAMSQ-asphaltenes composite particles in crude oil, thus improving the flowability of crude oil by inducing the mutual aggregation of wax crystals and compacting the morphology of wax crystal aggregations.

3.5.2. *Effect of T_{pre} on the wax deposition characteristics of the undoped/doped crude oil*

It can be seen from Section 3.3 that as T_{pre} increases, the wax deposition rate of the doped crude oil gradually decreases, but the average wax content of the formed wax deposits gradually increases. This is mainly due to the gradual improvement of the low-temperature flowability of crude oil as T_{pre} increases, and this is beneficial to the diffusion of wax molecules. On the other hand, the aging rate of wax deposits accelerates, and the average wax content of wax deposits increases.

As shown in section 3.3.1, when T_{pre} is 50 °C, the wax inhibitor

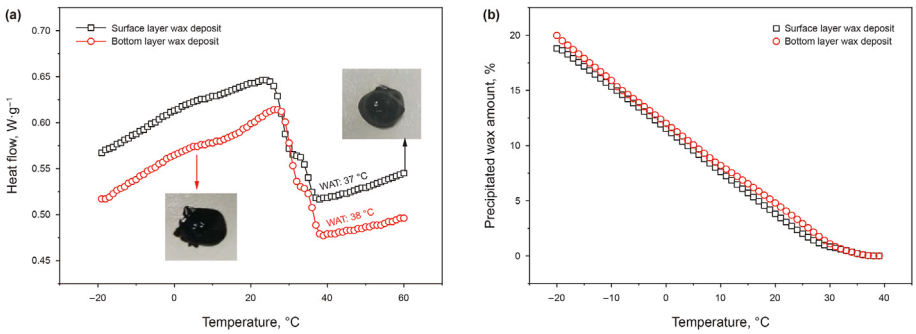

Fig. 10. The DSC curve of wax deposit formed by the doped crude oil at T_{pre} = 50 °C after 6 h: (**a**) the exothermic characteristics; (**b**) the precipitated wax amount.

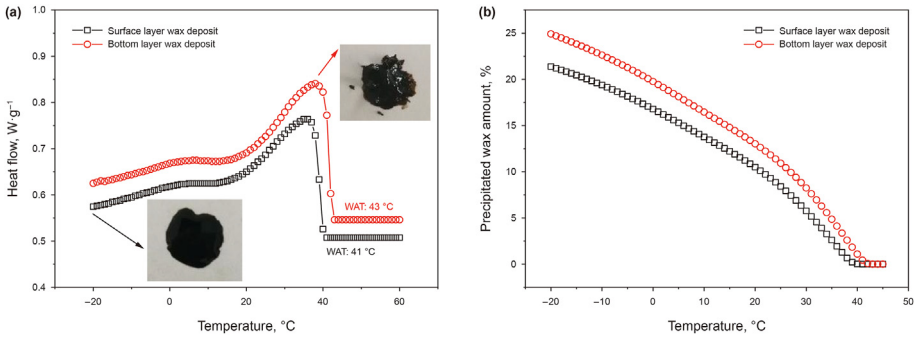

Fig. 11. The DSC curve of wax deposit formed by the doped crude oil at T_{pre} = 60 °C after 6 h: (**a**) the exothermic characteristics; (**b**) the precipitated wax amount.

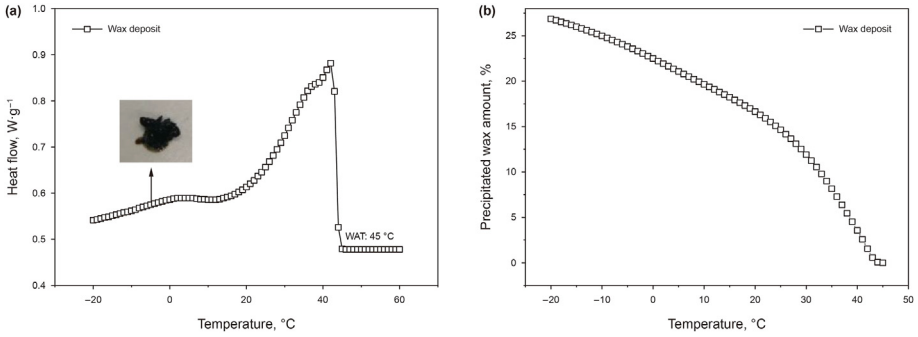

Fig. 12. The DSC curve of wax deposit formed by the doped crude oil at T_{pre} = 70 °C after 6 h: (**a**) the exothermic characteristics; (**b**) the precipitated wax amount.

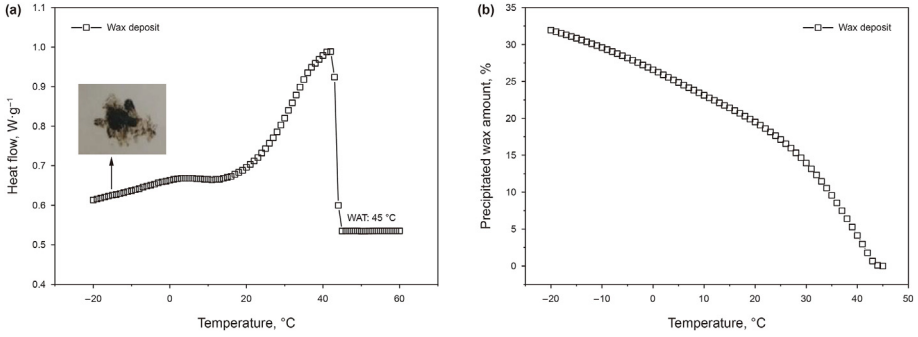

Fig. 13. The DSC curve of wax deposit formed by the doped crude oil at T_{pre} = 80 °C after 6 h: (**a**) the exothermic characteristics; (**b**) the precipitated wax amount.

cannot inhibit the wax deposition rate and cannot increase the wax content of the formed wax deposit. Because at this pre-heating treatment temperature, the wax inhibitor has no significant effect on the crude oil viscosity and low-temperature gel structure strength and basically does not affect the wax crystal morphology and crystallization exothermic characteristics of the crude oil. These parameters are the main factors related to the wax deposition process. When T_{pre} is higher than 60 °C, the addition of wax inhibitors has a significant wax inhibition effect on the crude oil and the wax inhibition efficiency decreases with the increase of T_{pre}. With the increase of T_{pre}, the addition of the wax inhibitor will increase the wax content of the wax deposit. It can be seen from Fig. 7 that at T_{pre} = 60 °C, the storage modulus of the undoped and doped crude oil are 1834.3 Pa and 0.201 Pa, respectively. With the increase of T_{pre} from 60 to 70 °C, the values changed to 119 and 0.7 Pa. At T_{pre} = 80 °C, the values changed to 1.1 and 0.7 Pa. The difference between the storage modulus of undoped and doped crude oil decreases with the increase of T_{pre}. The wax deposit mass is mainly controlled by the gel structure strength of the bulk oil near the pipe wall. During the wax deposition process, the stronger low-temperature gel structure strength is conducive to the adhesion and growth of the wax deposits. At T_{pre} = 60 °C, the difference in the gel structure strength between undoped and doped crude oil is the largest, so the difference in wax deposit mass between undoped and doped crude oil is the largest. With the gradual increase of T_{pre}, the difference between the gel structure of undoped and doped crude oil gradually decreases. The difference in wax deposit mass is decreased due to the increase of pre-heating treatment temperature, which causes a decrease of wax inhibition efficiency.

4. Conclusion

The rheological and wax deposition experiments at different pre-heating treatment temperatures (T_{pre}) were carried out thoroughly here to study the pre-heating temperature induced

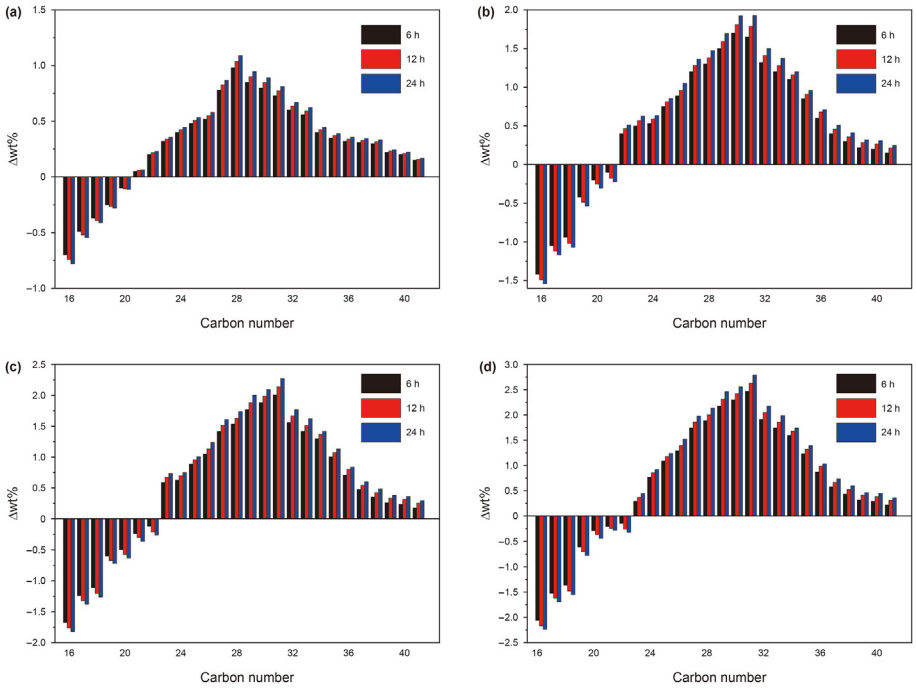

Fig. 14. Development of the *n*-alkane composition of the doped crude oil wax deposits with time (**a**) 50 °C outer-layer; (**b**) 60 °C outer-layer; (**c**) 70 °C; (**d**) 80 °C.

flowability and wax deposition characteristics of crude oil adding wax inhibitors. It is found that as T_{pre} increases, the solvation effect is strengthened and the asphaltenes/resins and wax inhibitors are better dispersed for stronger interactions between wax inhibitors and asphaltenes/resins, which decreases the quality of doped wax deposit while increases the wax content of wax deposit. The main mechanism was concluded that T_{pre} increase improves the low-temperature gelling structure strength of crude oil, which is unfavorable to the adhesion of wax deposits on the wall, and increases the solid wax concentration required for the formation of wax deposits on the wall, and the improvement of fluidity is also conducive to the aging of wax deposits.

Declaration of competing interest

The authors declare the following financial interests/personal relationships which may be considered as potential competing interests:

Bo Yao reports financial support was provided by National Natural Science Foundation of China.

Acknowledgement

The authors thank the financial support from the National Natural Science Foundation of China (51904327, U19B2012) and China University of Petroleum Innovation Project (22CX06050A).

Appendix A. Supplementary data

Supplementary data to this article can be found online at https://doi.org/10.1016/j.petsci.2023.02.030.

References

Aiyejina, A., Chakrabarti, D.P., Pilgrim, A., Sastry, M., 2011. Wax formation in oil pipelines: a critical review. Int. J. Multiphas. Flow 37 (7), 671–694. https://doi.org/10.1016/j.ijmultiphaseflow.2011.02.007.

Chala, G.T., Sulaiman, S.A., Japper-Jaafar, A., 2018. Flow start-up and transportation of waxy crude oil in pipelines-A review. J. Non-Newtonian Fluid Mech. 251, 69–87. https://doi.org/10.1016/j.jnnfm.2017.11.008.

Chen, C., Zhang, J., Ma, C., et al., 2019. Influence of wax precipitation on the impedance spectroscopy of waxy oils. Energy Fuel. 33 (10), 9767–9778. https://doi.org/10.1021/acs.energyfuels.9b02543.

Chi, Y., Daraboina, N., Sarica, C., 2016. Investigation of inhibitors efficacy in wax deposition mitigation using a laboratory scale flow loop. AIChE J. 62 (11), 4131–4139. https://doi.org/10.1002/aic.15307.

Chi, Y., Daraboina, N., Sarica, C., 2017. Effect of the flow field on the wax deposition and performance of wax inhibitors: cold finger and flow loop testing. Energy Fuel. 31 (5), 4915–4924. https://doi.org/10.1021/acs.energyfuels.7b00253.

Dorsman, I.R., Chan, D.H.H., Cunningham, V.J., et al., 2022. Synthesis of crystallizable poly (behenyl methacrylate)-based block and statistical copolymers and their performance as wax crystal modifiers. Polym. Chem. 13 (41), 5861–5872. https://doi.org/10.1039/d2py01023b.

Evdokimov, I.N., Eliseev, N.Y., Eliseev, D.Y., 2003. Thermophysical properties and phase-behaviour of asphaltene-containing petroleum fluids. Fluid Phase Equil. 212 (1–2), 269–278. https://doi.org/10.1016/S0378-3812(03)00267-X.

Fan, K., Li, S., Li, R., 2021. Development of wax molecular diffusivity correlation suitable for crude oil in wax deposition: experiments with a cold-finger apparatus. J. Petrol. Sci. Eng. 205, 108851. https://doi.org/10.1016/j.petrol.2021.108851.

Giacchetta, G., Marchetti, B., Leporini, M., et al., 2019. Pipeline wax deposition modeling: a sensitivity study on two commercial software. Petroleum 5 (2), 206–213. https://doi.org/10.1016/j.petlm.2017.12.007.

Janamatti, A., Lu, Y., Ravichandran, S., et al., 2019. Influence of operating temperatures on long-duration wax deposition in flow lines. J. Petrol. Sci. Eng. 183, 106373. https://doi.org/10.1016/j.petrol.2019.106373.

Jafari Ansaroudi, H., Vafaie-Sefti, M., Masoudi, S., Behbahani, T.J., Jafari, H., 2013. Study of the morphology of wax crystals in the presence of ethylene-co-vinyl acetate copolymer. Petrol. Sci. Technol. 31 (6), 643–651. https://doi.org/10.1080/10916466.2011.632800.

Jennings, D.W., Weispfennig, K., 2005. Effects of shear and temperature on wax deposition: coldfinger investigation with a Gulf of Mexico crude oil. Energy Fuel. 19 (4), 1376–1386. https://doi.org/10.1021/ef049784i.

Kang, P.S., Hwang, J.Y., Lim, J.S., 2019. Flow rate effect on wax deposition behavior in single-phase laminar flow. J. Energy Resour. Technol. 141 (3). https://doi.org/10.1115/1.4041525.

Kurniawan, M., Ruwoldt, J., Norrman, J., et al., 2021. Influence of wax inhibitor molecular weight on solution crystallization and rheology of monodisperse waxes. Energy Fuel. 35 (9), 7666–7680. https://doi.org/10.1021/acs.energyfuels.0c04187.

Leporini, M., Terenzi, A., Marchetti, B., et al., 2019. Experiences in numerical simulation of wax deposition in oil and multiphase pipelines: theory versus reality. J. Petrol. Sci. Eng. 174, 997–1008. https://doi.org/10.1016/j.petrol.2018.11.087.

Li, R., Huang, Q., Zhu, X., Zhang, D., Lv, Y., Larson, R.G., 2021. Investigation of delayed formation of wax deposits in polyethylene pipe using a flow-loop. J. Petrol. Sci.

Eng. 196, 108104. https://doi.org/10.1016/j.petrol.2020.108104.
Li, W., Li, H., Da, H., et al., 2021. Influence of pour point depressants (PPDs) on wax deposition: a study on wax deposit characteristics and pipeline pigging. Fuel Process. Technol. 217, 106817. https://doi.org/10.1016/j.fuproc.2021.106817.
Mansourpoor, M., Azin, R., Osfouri, S., et al., 2019. Experimental investigation of wax deposition from waxy oil mixtures. Applied Petrochemical Research 9, 77–90. https://doi.org/10.1007/s11053-019-09454-z.
Makwashi, N., Zhao, D., Abdulkadir, M., Ahmed, T., Muhammad, I., 2021. Study on waxy crudes characterisation and chemical inhibitor assessment. J. Petrol. Sci. Eng. 204, 108734. https://doi.org/10.1016/j.petrol.2021.108734.
Martos, C., Coto, B., Espada, J.J., et al., 2008. Experimental determination and characterization of wax fractions precipitated as a function of temperature. Energy Fuel. 22 (2), 708–714. https://doi.org/10.1021/ef7003927.
Qing, M., Lei, S., 2004. Study on the wax deposition law for daqing crude oil treated with PPD. Oil Gas Storage Transp. 23 (7), 53–70. https://doi.org/10.3321/j.issn:0253-2697.2006.04.028, 58+65.
Ragunathan, T., Husin, H., Wood, C.D., 2020. Wax formation mechanisms, wax chemical inhibitors and factors affecting chemical inhibition. Appl. Sci. 10 (2), 479. https://doi.org/10.3390/app10020479.
Ruwoldt, J., Sørland, G.H., Simon, S., et al., 2019. Inhibitor-wax interactions and PPD effect on wax crystallization: new approaches for GC/MS and NMR, and comparison with DSC, CPM, and rheometry. J. Petrol. Sci. Eng. 177, 53–68. https://doi.org/10.1016/j.petrol.2019.02.046.
Ruwoldt, J., Kurniawan, M., Oschmann, H.J., 2018. Non-linear dependency of wax appearance temperature on cooling rate. J. Petrol. Sci. Eng. 165, 114–126. https://doi.org/10.1016/j.petrol.2018.02.011.
Singh, P., Venkatesan, R., Fogler, H.S., Nagarajan, N., 2000. Formation and aging of incipient thin film wax-oil gels. AIChE J. 46 (5), 1059–1074. https://doi.org/10.1002/aic.690460517.
Sousa, A.M., Matos, H.A., Guerreiro, L., 2020. Wax deposition mechanisms and the effect of emulsions and carbon dioxide injection on wax deposition: critical review. Petroleum 6 (3), 215–225. https://doi.org/10.1016/j.petlm.2019.09.004.
Sousa, A., Matos, H., Guerreiro, L., 2019. Preventing and removing wax deposition inside vertical wells: a review. J. Pet. Explor. Prod. Technol. 9 (3), 2091–2107. https://doi.org/10.1007/s13202-019-0609-x.
Sun, M., Naderi, K., Firoozabadi, A., 2019. Effect of crystal modifiers and dispersants on paraffin-wax particles in petroleum fluids. SPE J. 24, 32–43. https://doi.org/10.2118/191365-PA, 01.
Wang, K.-S., Wu, C.-H., Creek, J.L., Shuler, P.J., Tang, Y., 2003. Evaluation of effects of selected wax inhibitors on paraffin deposition. Petrol. Sci. Technol. 21 (3–4), 369–379. https://doi.org/10.1081/LFT-120018526.
Wong, G.K., Yen, T.F., 2000. An electron spin resonance probe method for the understanding of petroleum asphaltene macrostructure. J. Petrol. Sci. Eng. 28 (1–2), 55–64. https://doi.org/10.1016/S0920-4105(00)00067-X.
Xu, Y., Huang, Q., 2010. Rheological property of waxy crude oil in restart process of pipeline[C]. International Pipeline Conference 44229, 399–403.
Yang, J., Lu, Y., Daraboina, N., Sarica, C., 2020. Wax deposition mechanisms: is the current description sufficient? Fuel 275, 117937. https://doi.org/10.1016/j.fuel.2020.117937.
Yang, F., Cai, J., Cheng, L., Li, C., Ji, Z., Yao, B., Zhao, Y., Zhang, G., 2016. Development of asphaltenes-triggered two-layer waxy oil gel deposit under laminar flow: an experimental study. Energy Fuel. 30 (11), 9922–9932. https://doi.org/10.1021/acs.energyfuels.6b01482.
Yang, F., Cheng, L., Liu, H., Yao, B., Li, C., Sun, G., Zhao, Y., 2018. Comb-like poly-octadecyl acrylate (POA) wax inhibitor triggers the formation of heterogeneous waxy oil gel deposits in a cylindrical Couette device. Energy Fuel. 32 (1), 373–383. https://doi.org/10.1021/acs.energyfuels.7b03416.
Yang, F., Zhu, H., Li, C., Yao, B., Wang, F., Chen, J., Sun, G., 2021. Investigation on the mechanism of wax deposition inhibition induced by asphaltenes and wax inhibitors. J. Petrol. Sci. Eng. 204, 108723. https://doi.org/10.1016/j.petrol.2021.108723.
Yao, B., Li, C., Zhang, X., Yang, F., Sun, g., Zhao, Y., 2018. Performance improvement of the ethylene-vinyl acetate copolymer (EVA) pour point depressant by small dosage of the amino-functionalized polymethylsilsesquioxane (PAMSQ) microsphere. Fuel 220, 167–176. https://doi.org/10.1016/j.fuel.2018.01.032.
Zhao, J., Xi, X., Dong, H., Li, Y., Jiang, M., 2021. In situ observation of microscopic motions and the structure dynamic transformation of wax crystals in waxy crude oil subjected to shear. New J. Chem. 45 (37), 17522–17543. https://doi.org/10.1039/d1nj02292j.
Zhu, H., Li, C., Yang, F., Liu, H., Liu, D., Sun, G., Yao, B., Liu, G., Zhao, Y., 2018. Effect of pre-heating treatment temperature on the flowability and wax deposition characteristics of Changqing waxy crude oil. Energy Fuel. 32 (10), 10605–10615. https://doi.org/10.1021/acs.energyfuels.8b02552.